

CrossADR: enhancing adverse drug reactions prediction for combination pharmacotherapy with cross-layer feature integration and cross-level associative learning

Y. Cheung^{1,*}

¹School of Mathematical Sciences and Shanghai Key Laboratory of PMMP, East China Normal University, 200241, Shanghai, China

*Corresponding author. 52275500001@stu.ecnu.edu.cn

Abstract

Combination pharmacotherapy offers substantial therapeutic advantages but also poses substantial risks of adverse drug reactions (ADRs). The accurate prediction of ADRs with interpretable computational methods is crucial for clinical safety management, drug development, and precision medicine. However, managing ADRs remains a challenge due to the vast search space of drug combinations and the complexity of physiological responses. Current graph-based architectures often struggle to effectively integrate multi-scale biological information and frequently rely on fixed association matrices, which limits their ability to capture dynamic organ-level dependencies and generalize across diverse datasets. Here we propose CrossADR, a hierarchical framework for organ-level ADR prediction through cross-layer feature integration and cross-level associative learning. It incorporates a gated-residual-flow graph neural network to fuse multi-scale molecular features and utilizes a learnable ADR embedding space to dynamically capture latent biological correlations across 15 organ systems. Systematic evaluation on the newly constructed CrossADR-Dataset—covering 1,376 drugs and 946,000 unique combinations—demonstrates that CrossADR consistently achieves state-of-the-art performance across 80 distinct experimental scenarios and provides high-resolution insights into drug-related protein interactions and pathways. Overall, CrossADR represents a robust tool for cross-scale biomedical information integration, cross-layer feature integration as well as cross-level associative learning, and can be effectively utilized to prevent ADRs in clinical decision-making.

Keywords adverse drug reactions, combination pharmacotherapy, cross-layer feature integration, cross-level associative learning, clinical drug safety

Introduction

Combination pharmacotherapy has emerged as a cornerstone of modern medicine due to its ability to provide complementary efficacy, alleviate toxicity, and delay the onset of drug resistance [1, 2, 3]. However, as compounds with inherent bioactivity, drugs often carry the risk of adverse drug reactions (ADRs), which are frequently exacerbated when multiple agents are administered together [4, 5, 6]. The accurate prediction of ADRs with interpretable computational methods is crucial for clinical safety management, drug development, and precision medicine [7, 8, 9]. Recently, OrganADR pioneered the ADRs study within drug-drug interaction research by emphasizing an organ perspective [10]. This shifted the focus from broad ADRs to localized physiological impacts, providing a crucial foundation for precise and manageable clinical safety assessments [11, 12].

Despite these conceptual advances, managing ADRs remains a monumental challenge due to the vast search space of drug combinations. With over 2,000 FDA-approved drugs, the potential pairings exceed one million, making it impossible to rely solely on clinical records or the experience of individual physicians across different medical departments [13, 14]. While computational methods have continuously improved, reports from OrganADR indicate that

ADR prediction accuracy at the organ level still hovers between 70% and 80%. This gap remains a substantial barrier to meeting the rigorous safety demands of clinical practice and drug management.

Current mainstream architectures typically rely on Knowledge Graphs and Graph Neural Networks (GNN-KG) [15, 16], yet they often overlook the natural physiological connections between organs. Although OrganADR addressed this by using an ADR association matrix, this approach relies heavily on large, unbiased training data. In real-world scenarios, such models risk learning data biases rather than true, interpretable biological information [17, 18]. Furthermore, while some studies have identified molecular-level and organ-level information within biomedical networks, they usually treat these layers as isolated modules linked only by simple attention mechanisms [19, 20]. Inspired by residual connections in computer science and biochemical cascades in life sciences, we argue that vital information exists across different scales and stages that previous models have failed to integrate fully. This lack of deep feature fusion serves as the primary computational motivation for our current study.

To address these gaps, CrossADR, a framework designed for organ-level ADR prediction through cross-layer feature integration and cross-level associative learning, is presented (Fig.1). The architecture utilizes four types of drug features processed through learnable

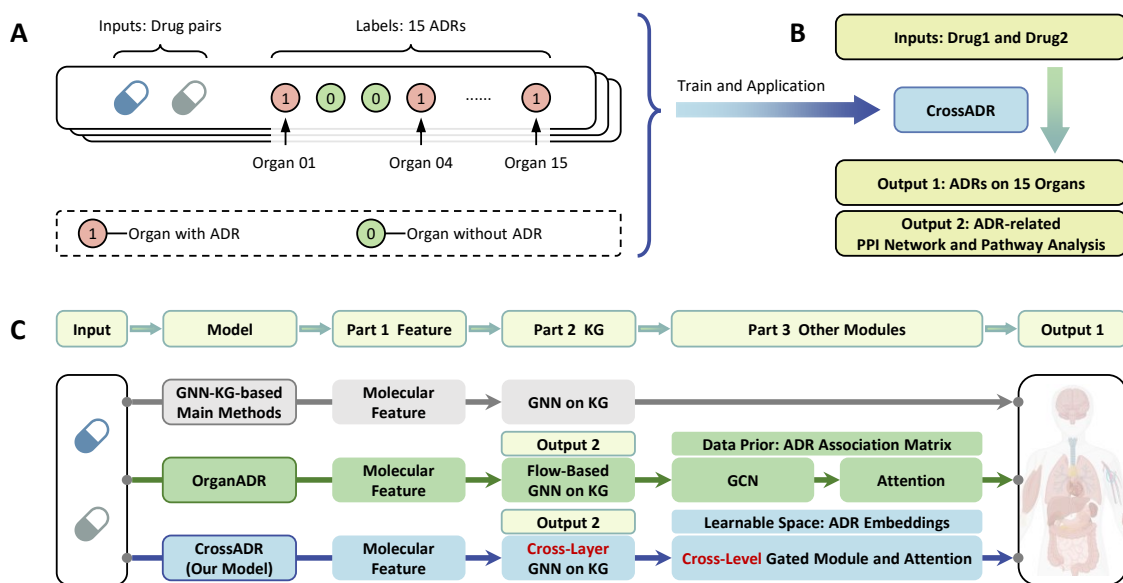


Figure 1 Overview of the CrossADR framework for organ-level adverse drug reaction (ADR) prediction. (A) Input: drug pairs, as well as the 15 ADR labels at organ level. (B) The training and application workflow of CrossADR for predicting ADRs and performing downstream PPI network and pathway analysis. (C) Architectural comparison between baseline methods (GNN-KG-based, OrganADR) and the proposed CrossADR model, highlighting two proposed important module: (1) the cross-layer feature integration module, (2) the learnable ADR embeddings as well as cross-level gated module and attention mechanisms.

self-attention modules. Specifically, it employs a cross-layer GNN on Knowledge Graphs that incorporates drug-dependent attention scores on edge types, a gated-residual-flow mechanism, and bi-directional cross-attention. Unlike previous methods, CrossADR abandons fixed association matrices in favor of a learnable space for ADR embeddings. This innovation allows the model to capture organ-level information dynamically, reducing sensitivity to data bias and improving generalization across different datasets. By focusing on the cross-layer fusion of molecular features within the biomedical network and cross-level integration between molecular and organ responses, the model achieves a more robust and associative learning process.

CrossADR is evaluated using the newly constructed CrossADR-Dataset, which covers 1,376 drugs and a vast combination space of 946,000 unique pairs, representing a significant expansion over previous benchmarks. Our evaluation spanned ten independent datasets across 80 distinct scenarios and 15 organ systems. Results show that CrossADR consistently achieves superior performance over both state-of-the-art deep learning models and widely used machine learning methods. Ablation studies further confirm the effectiveness of our architectural innovations, particularly the gated modules and multi-scale fusion. Finally, case studies demonstrate that CrossADR can identify drug-related and ADR-related protein interactions and pathways [21]. Given the massive scale of potential drug combinations and the large patient populations affected by multi-morbidity, the performance gains and biological insights provided by CrossADR offer significant value for clinical drug management and patient safety.

Methods

Problem formulation of ADR prediction

Following ref.[10], the objective of this study is to predict the potential adverse drug reactions (ADRs) that arise when two specific drugs, denoted as p and q , are administered together. As illustrated

in Fig.1a-b, the set of ADRs for this drug pair is defined as follows:

$$\mathcal{A}_{p,q} = \{a_{p,q}^i\}, \quad i = 1, 2, \dots, 15, \quad (1)$$

In this formulation, the disordered collection of side effects observed under the combined pharmacotherapy of p and q is represented by $\mathcal{A}_{p,q}$, where the index i corresponds to a specific organ system.

For each individual organ, the occurrence of an ADR is captured by a binary value. The specific status of an ADR is determined by:

$$a_{p,q}^i = \begin{cases} 1, & \text{if an ADR is caused in organ } i \text{ by } p + q \\ 0, & \text{if no ADR is caused in organ } i \text{ by } p + q \end{cases}. \quad (2)$$

where value of 1 is assigned if an ADR is triggered. Conversely, a value of 0 is recorded if the organ remains unaffected by $p + q$.

CrossADR focus on "Predict ADRs between two emerging drugs", with the same task formulation in [10, 22], as shown in Fig.2a.

Model: architecture of CrossADR

In summary, the architecture of CrossADR establishes a hierarchical information processing pipeline that transitions from microscopic molecular structures to macroscopic organ-level responses. By integrating diverse drug features with prior knowledge from the PrimeKG, the model employs a gated-residual-flow GNN and bi-directional cross-attention to capture the multi-scale evolution of drug-drug interactions. Furthermore, the introduction of a learnable ADR embedding space and cross-level attention mechanisms enables the model to adaptively fuse molecular-level network signals with latent biological correlations between organ systems. This synergistic design ensures that CrossADR can model the complex, non-linear dependencies inherent in multi-organ ADR predictions, providing a robust and interpretable framework for drug safety assessment.

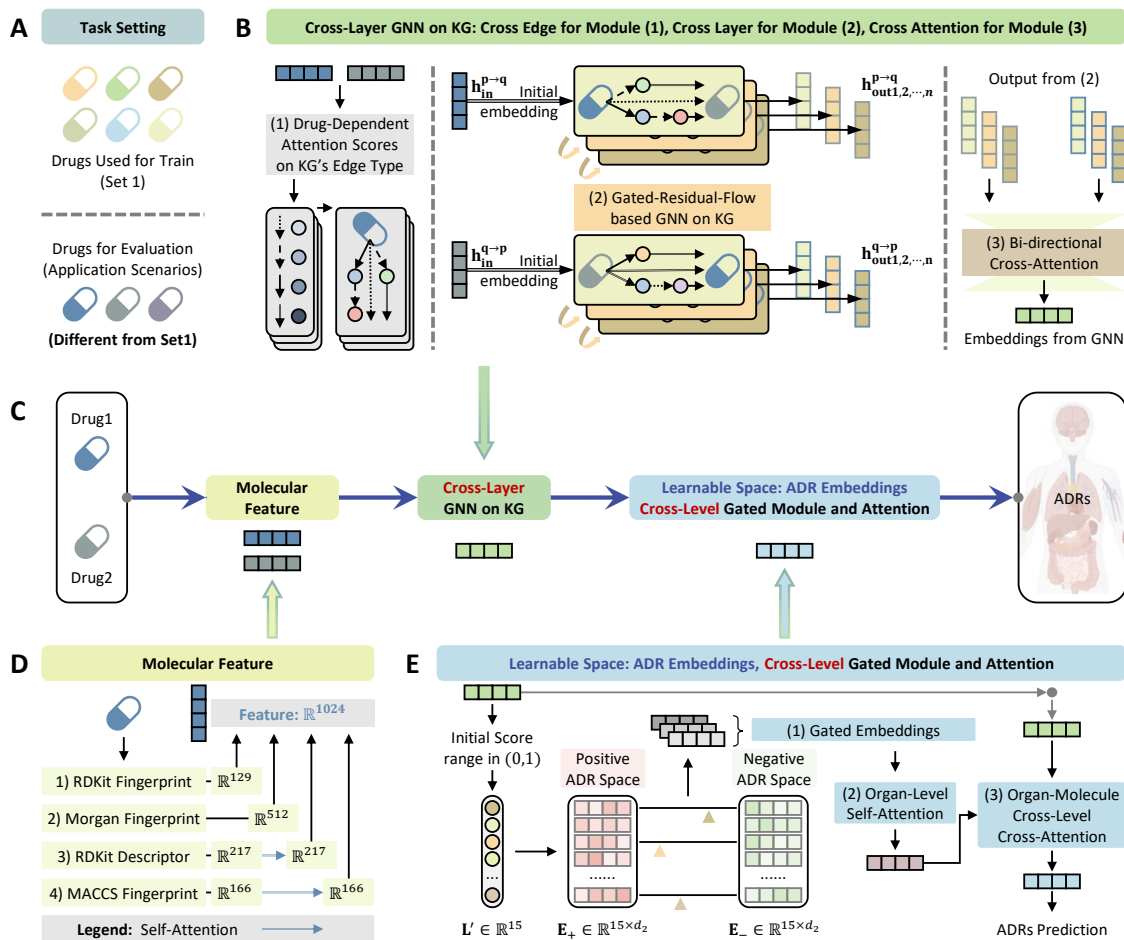


Figure 2 Detailed architecture of CrossADR. (A) Task setting for “emerging drug -emerging drug” ADR prediction task. (B) The cross-layer GNN on KG module. (C) The workflow of CrossADR. (D) Molecular feature. (E) The cross-level gated module and attention module with learnable ADR embedding space.

Molecular feature

The innovation of CrossADR lies in its architecture. Therefore, for drug representation, CrossADR applies the same features as OrganADR[10]. The extraction process begins with the generation of initial feature vectors for each drug, denoted as $\mathbf{f}_p \in \mathbb{R}^{1024}$ and $\mathbf{f}_q \in \mathbb{R}^{1024}$, as shown in Fig.2d. In this phase, one molecular descriptor and three distinct types of molecular fingerprints are extracted. Since the components of the RDKit descriptors and MACCS fingerprints represent specific physical or chemical properties—such as molecular weight or the count of carbon atoms—two independent, trainable self-attention modules are utilized to process them.

For each feature type \mathbf{x}_k that requires attention, a weight vector \mathbf{w}_k is calculated to capture the importance of different dimensions:

$$\mathbf{w}_k = \text{Softmax}(\mathbf{W}_k \mathbf{x}_k), \quad \mathbf{e}_k = \mathbf{x}_k \odot \mathbf{w}_k, \quad (3)$$

where \mathbf{W}_k denotes the trainable weight matrix of the linear layer, and \odot represents the Hadamard product used for element-wise weighting.

Specifically, four kinds of drug features applied for CrossADR are:

- Continuous molecular descriptors are calculated via the “CalcMolDescriptors” function in RDKit. These descriptors are used to quantify essential physicochemical properties, such as the molecular weight, and the polar surface area (PSA).

- Path-based fingerprints are generated using the “RDKit Fingerprint” function. This is included because the structure and substructure of drugs are identified as critical factors for predicting drug-drug interactions in several studies[23, 24, 25].
- MACCS keys are employed to provide a clear characterization of key molecular substructures. Through this method, features such as ring structures, element types, and the presence of rare atoms are explicitly encoded into one-hot vectors.
- Morgan fingerprints (radius is set to 2) are utilized to represent the local atomic environment. The molecular structure is encoded by considering the specific neighborhood around each atom, ensuring that subtle structural differences are captured.

Knowledge graph

Knowledge graph provides the foundational data structure for models’ graph convolutional modules and also provides prior biomedical network knowledge for the ADR prediction task. As illustrated in Fig.3, four node types from PrimeKG are retained, along with their corresponding edges. To ensure the integrity of the evaluation, “synergistic interaction” edges between drugs are removed from PrimeKG to prevent knowledge leakage. Furthermore, bi-directional connections in PrimeKG are filtered into uni-directional

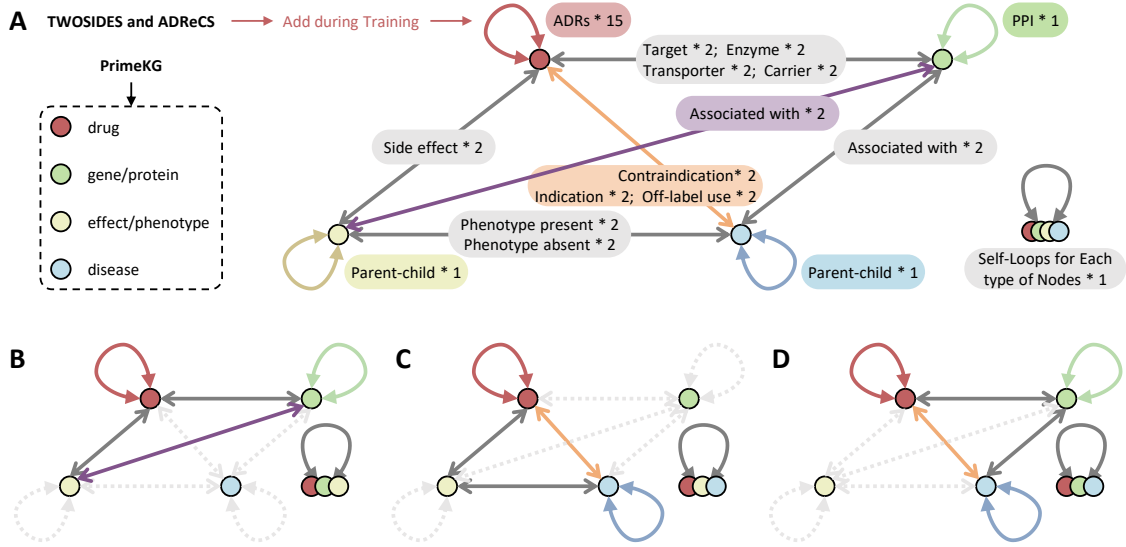


Figure 3 Knowledge Graph (KG) construction and ablated KGs. (A) Integration of TWOSIDES and ADReCS, as well as the topology of the basic KG. (B,C,D) Three ablated KGs for comparison. B, C and D for ablated KG 1, 2 and 3. Based on the basic KG, different type of information is removed accordingly.

interactions that are biologically justified. Detailed edge types and statistics for the knowledge graphs are provided in Table.2.

GNN module: Cross-layer GNN on KG

Following ref.[22, 10], a flow-based GNN module, which represents a state-of-the-art architecture in DDI prediction, is employed to generate embedding vectors for each drug pair. However, CrossADR innovatively captures features more comprehensively through (1) drug-dependent attention scores on KG edge types, (2) a gated-residual-flow-based GNN on the KG, and (3) bi-directional cross-attention, as illustrated in Fig.2b. Let \mathbf{f}_p and \mathbf{f}_q to represent the molecular features extracted for drugs p and q , respectively, the output of the cross-layer GNN module can be summarized as follows:

$$\mathbf{h}_{out1}^{p,q} = f_{GNN}(\mathcal{G}, \mathbf{f}_p, \mathbf{f}_q). \quad (4)$$

The cross-layer GNN propagates information across L layers. For each layer $l \in \{1, \dots, L\}$, the module first computes drug-dependent relation attention weights $\alpha_r^{(l)}$ based on the drug pair context:

$$\alpha_r^{(l)} = \sigma \left(\mathbf{W}_{attn}^{(l)} \cdot \text{ReLU} \left(\mathbf{W}_{rel}^{(l)} [\mathbf{f}_p; \mathbf{f}_q] \right) \right), \quad (5)$$

where $\mathbf{W}_{rel}^{(l)}$ and $\mathbf{W}_{attn}^{(l)}$ are learnable weight matrices, which scale the relation embeddings $\mathbf{r}^{(l)}$ to form the relation-aware message:

$$\hat{\mathbf{r}}^{(l)} = \alpha_r^{(l)} \odot \mathbf{r}^{(l)}. \quad (6)$$

In the l -th layer of the GNN module, the representation of an entity e in the flow starting from p toward q (denoted as $\mathbf{h}_{p,e}^{(l)}$) is updated using a message-passing mechanism on the KG \mathcal{G} :

$$\tilde{\mathbf{h}}_{p,e}^{(l)} = \text{ReLU} \left(\mathbf{W}^{(l)} \sum_{e' \in \mathcal{N}(e)} (\mathbf{h}_{p,e'}^{(l-1)} \odot \hat{\mathbf{r}}_{e',e}^{(l)}) \right), \quad (7)$$

where $\mathcal{N}(e)$ denotes the neighbors of e in \mathcal{G} .

To mitigate numerical oversmoothing and structural feature homogenization, a gated-residual-flow mechanism is implemented,

whereby the initial drug features are preserved throughout the propagation. The hidden state is updated via a gating weight $g^{(l)}$:

$$g^{(l)} = \sigma \left(\mathbf{W}_{gate}^{(l)} [\tilde{\mathbf{h}}_{p,e}^{(l)}; \mathbf{h}_{p,e}^{(0)}] \right), \quad (8)$$

and

$$\mathbf{h}_{p,e}^{(l)} = g^{(l)} \cdot \tilde{\mathbf{h}}_{p,e}^{(l)} + (1 - g^{(l)}) \cdot \mathbf{h}_{p,e}^{(0)}, \quad (9)$$

where $\mathbf{h}_{p,e}^{(0)} = \mathbf{f}_p$ is the initial drug feature from the previous module.

In contrast to conventional architectures that are restricted to final-layer representations, a multi-scale feature fusion strategy is adopted by CrossADR, whereby the latent embeddings of target drugs are extracted at each layer to capture the hierarchical evolution of knowledge flow. For the pair (p, q) , we obtain sequences of latent vectors $\mathbf{H}_p = \{\mathbf{h}_{p,q}^{(1)}, \dots, \mathbf{h}_{p,q}^{(L)}\}$ and $\mathbf{H}_q = \{\mathbf{h}_{q,p}^{(1)}, \dots, \mathbf{h}_{q,p}^{(L)}\}$. Based on the above architecture, in order to effectively fuse these multi-layer features, bi-directional cross-attention is then applied:

$$\mathbf{A} = \text{Softmax} \left(\frac{(\mathbf{W}_{cross} \mathbf{H}_p) \mathbf{H}_q^T}{\sqrt{d}} \right), \quad (10)$$

The cross-attended representations are calculated as $\hat{\mathbf{H}}_p = \mathbf{A} \mathbf{H}_q$ and $\hat{\mathbf{H}}_q = \mathbf{A}^T \mathbf{H}_p$. Finally, the output of the cross-layer GNN module $\mathbf{h}_{out1}^{p,q}$ is the concatenation of the flattened attended sequences:

$$\mathbf{h}_{out1}^{p,q} = [\text{vec}(\hat{\mathbf{H}}_p); \text{vec}(\hat{\mathbf{H}}_q)], \quad (11)$$

where $\mathbf{h}_{out1}^{p,q} \in \mathbb{R}^{2 \cdot L \cdot d_1}$, capturing the complex inter-dependencies between drugs across different hop-distances in the KG.

Cross-level attention module: Learnable space for ADR Embeddings

The embedded vector $\mathbf{h}_{out1}^{p,q}$ captures information at the molecular level and network-based interactions. To integrate the latent organ-level ADR associations, CrossADR introduces a learnable embedding space for ADR labels. Unlike fixed categorical representations, this

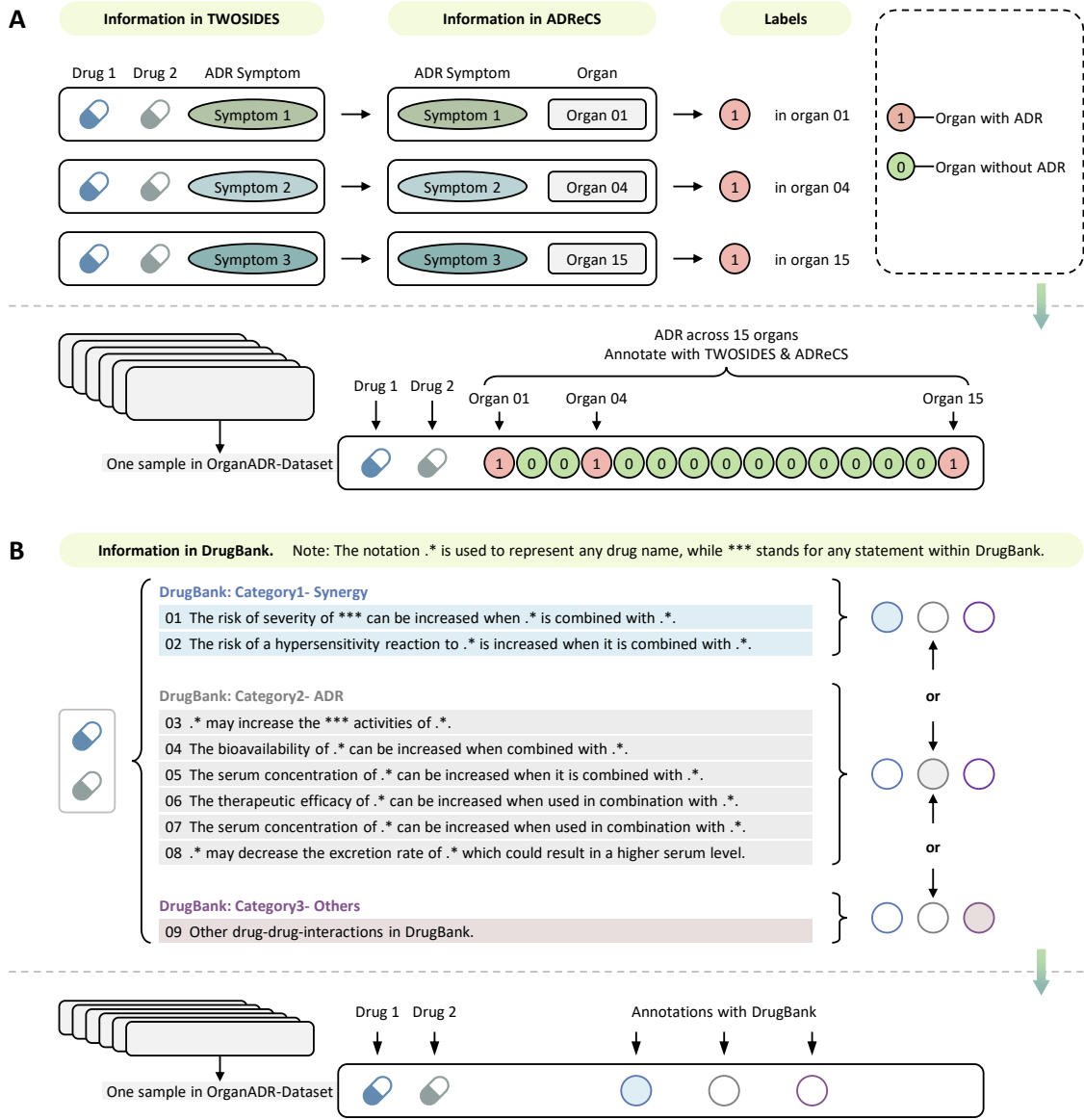


Figure 4 Data annotation and sample generation for the CrossADR-Dataset. (A) Mapping drug combinations from TWOSIDES and ADReCS to 15 specific organs to create multi organ ADR labels. (B) Integration of synergistic and ADR-related information from DrugBank to define positive and negative samples.

module maps drug-pair features into a multi-organ response space through a hierarchical attention mechanism.

Initially, $\mathbf{h}_{out1}^{p,q}$ is projected to generate preliminary ADR probability scores $\mathbf{S}_1 \in \mathbb{R}^{15}$ for the 15 organ categories:

$$\mathbf{S}_1 = \sigma(\mathbf{W}_{rel1}(\mathbf{h}_{out1}^{p,q}) + \mathbf{b}_{rel1}), \quad (12)$$

where $\mathbf{W}_{rel1} \in \mathbb{R}^{15 \times 2dL}$ and \mathbf{b}_{rel1} are learnable parameters.

To represent the presence or absence of ADRs in a continuous space, two learnable embedding sets are defined: the Positive ADR Space $\mathbf{E}_+ \in \mathbb{R}^{15 \times d_2}$ and the Negative ADR Space $\mathbf{E}_- \in \mathbb{R}^{15 \times d_2}$, where d_2 is the dimension of the organ embeddings. For organ i , the score $\mathbf{S}_1(i)$ acts as a gating signal to fuse the previous latent representations, forming the Gated Embeddings $\mathbf{H}_{initial} \in \mathbb{R}^{15 \times d_2}$:

$$g_i = \sigma(\mathbf{S}_1(i)), \quad (13)$$

and

$$\mathbf{H}_{initial}^{(i)} = g_i \cdot \mathbf{E}_+(i, :) + (1 - g_i) \cdot \mathbf{E}_-(i, :), \quad (14)$$

where σ denotes the sigmoid activation. This allows the model to capture the uncertainty and intensity of potential ADRs across different systems. Then, to model the complex co-occurrence and biological correlations between different organ systems, organ-level self-attention is applied on the initial gated features:

$$\mathbf{H}_{attn} = \text{MultiHeadAttention}(\mathbf{H}_{initial}, \mathbf{H}_{initial}, \mathbf{H}_{initial}), \quad (15)$$

$$\mathbf{H}_{refined} = \tanh(\mathbf{H}_{initial} + \mathbf{H}_{attn}). \quad (16)$$

The final organ-level feature vector $\mathbf{h}_{out2}^{p,q}$ is obtained by a weighted pooling based on the scores \mathbf{S}_1 and a global mean residual:

$$\mathbf{w}_{pool} = \text{Softmax}(\mathbf{S}_1), \quad (17)$$

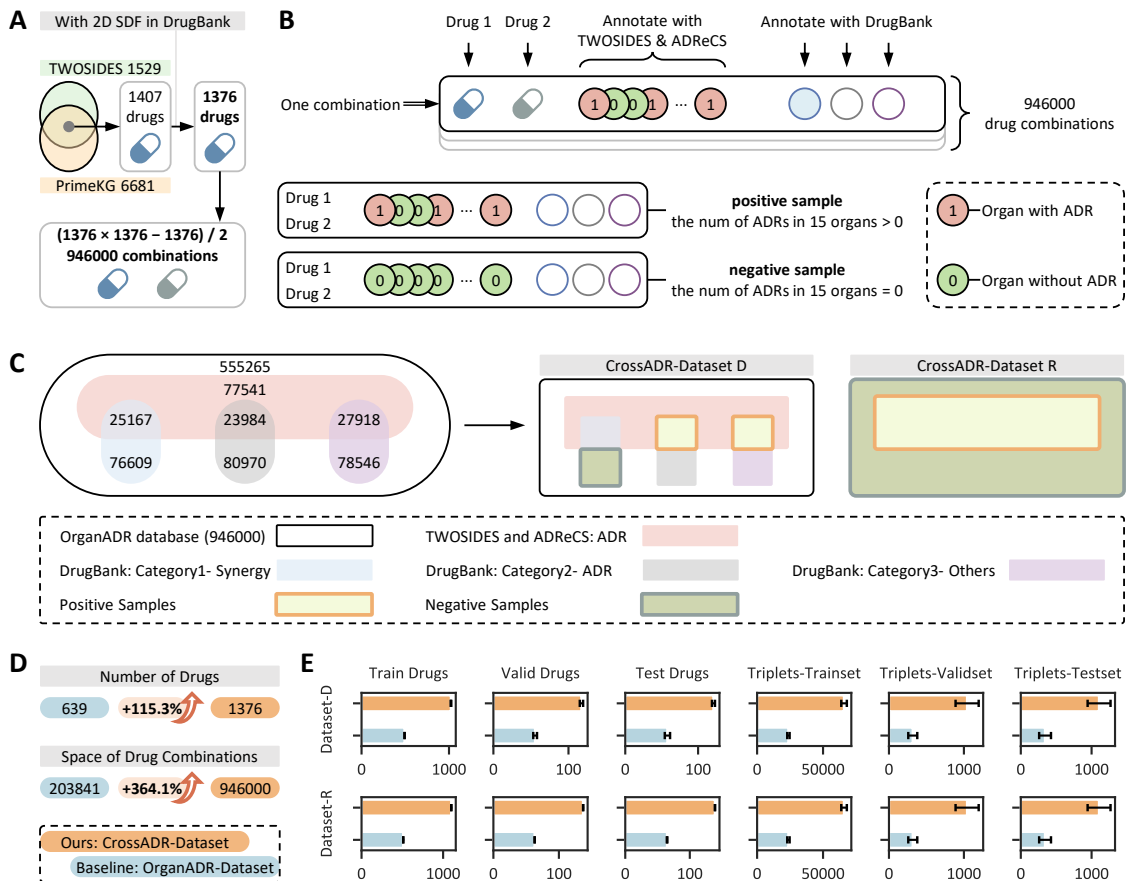


Figure 5 Construction and statistics of the CrossADR-Dataset. (A) Determine the drugs to be analyzed for CrossADR. (B) Construction of one sample (one drug combination and its annotations); definition of positive sample and negative sample. (C) CrossADR database, CrossADR-Dataset D and CrossADR-Dataset R. (D, E) Comparison of the number of drugs, total combination space and other metrics between OrganADR-Dataset and the proposed CrossADR-Dataset.

and

$$\mathbf{h}_{out2}^{p,q} = \sum_{i=1}^{15} (\mathbf{w}_{pool}(i) \cdot \mathbf{H}_{refined}(i, :)) + \text{Mean}(\mathbf{H}_{initial}). \quad (18)$$

Finally, to effectively fuse the molecular-level network features $\mathbf{h}_{out1}^{p,q}$ with the organ-level latent features $\mathbf{h}_{out2}^{p,q}$, an organ-molecule cross-level cross-attention mechanism is applied.

First, the organ feature $\mathbf{h}_{out2}^{p,q}$ is projected into the molecular feature space using a transformation matrix $\mathbf{W}_t \in \mathbb{R}^{2dL \times d_2}$:

$$\mathbf{h}_{out2}^{p,q'} = \mathbf{W}_t \mathbf{h}_{out2}^{p,q}. \quad (19)$$

The attention weights are then calculated by measuring the element-wise interaction between the molecular embedding and the transformed organ embedding, following the equations below:

$$\mathbf{A}_{score} = \mathbf{h}_{out1}^{p,q} \odot \mathbf{h}_{out2}^{p,q'}, \quad (20)$$

and

$$\mathbf{A}_{weight} = \text{Softmax}(\mathbf{A}_{score}). \quad (21)$$

Cross-level weighted representation $\mathbf{h}_{out3}^{p,q} \in \mathbb{R}^{2dL}$ is computed as:

$$\mathbf{h}_{out3}^{p,q} = \mathbf{A}_{weight} \odot \mathbf{h}_{out1}^{p,q}. \quad (22)$$

Finally, to make the final prediction, the original molecular flow features, the global organ latent features, and the cross-attended features would be concatenated as $\mathbf{E} \in \mathbb{R}^{4dL+d_2}$:

$$\mathbf{E} = [\mathbf{h}_{out1}^{p,q}; \mathbf{h}_{out2}^{p,q}; \mathbf{h}_{out3}^{p,q}]. \quad (23)$$

The final prediction scores $\mathbf{S} \in \mathbb{R}^{15}$ for ADRs in each organ or system are obtained through an output linear layer:

$$\mathbf{S} = \sigma(\mathbf{W}_{output} \mathbf{E} + \mathbf{b}_{output}), \quad (24)$$

Table 1 **Statistic of the CrossADR-Dataset.** The symbols $|\mathcal{D}_{\text{train}}|$, $|\mathcal{D}_{\text{valid}}|$, and $|\mathcal{D}_{\text{test}}|$ in the main manuscript represent Train/Valid/Test drug sets (in the table header), respectively. The symbols $|\mathcal{C}_{\text{train}}|$, $|\mathcal{C}_{\text{valid}}|$, and $|\mathcal{C}_{\text{test}}|$ in the main manuscript represent the Triplets in the Trainset/Validset/Testset (in the table header). Each triplet refers to a single sample, with a balanced 1 : 1 ratio between positive and negative samples.

Type	Seed	Train Drugs	Valid Drugs	Test Drugs	Triplets-Trainset	Triplets-Validset	Triplets-Testset
CrossADR-Dataset D	10	1022	119	121	64190	1118	1240
	15	1017	120	122	64826	1160	1142
	20	1021	117	119	64224	1040	1234
	25	1023	119	123	65070	1260	1032
	30	1028	115	119	62922	1234	1318
	35	1020	120	122	68636	956	798
	40	1020	118	125	65282	1016	1264
	45	1021	116	119	66854	1010	1016
	50	1026	115	119	68672	834	970
	55	1027	114	122	68572	802	1046
CrossADR-Dataset R	10	1100	137	139	64190	1118	1240
	15	1100	137	139	64826	1160	1142
	20	1100	137	139	64224	1040	1234
	25	1100	137	139	65070	1260	1032
	30	1100	137	139	62922	1234	1318
	35	1100	137	139	68636	956	798
	40	1100	137	139	65282	1016	1264
	45	1100	137	139	66854	1010	1016
	50	1100	137	139	68672	834	970
	55	1100	137	139	68572	802	1046

where $\mathbf{W}_{\text{output}} \in \mathbb{R}^{15 \times (4dL+d_2)}$. Using a threshold of 0.5, the final binary ADR prediction $\hat{A}_{p,q}$ is generated:

$$\hat{a}_{p,q}^i = \begin{cases} 1 & \text{if } \mathbf{S}_i \geq 0.5 \\ 0 & \text{if } \mathbf{S}_i < 0.5 \end{cases}, \quad i = 1, 2, \dots, 15. \quad (25)$$

Dataset: raw datasets and construction of CrossADR-Dataset

Raw datasets

For the accurate prediction of organ-level adverse drug reactions (ADRs) within emerging combination therapies, TWOSIDES [26] is utilized as the primary and most exhaustive database. Comprehensive prior knowledge is established through the biomedical knowledge graph, PrimeKG [27]. During the phase of data processing, ADReCS [28] is implemented to ensure that adverse drug reactions are mapped to organs. Furthermore, DrugBank [29] is employed for the annotation of drug combinations. Within this framework, DrugBank IDs (DBxxxxx) are systematically cross-referenced and matched to alternative identifiers to maintain data consistency.

Construction of CrossADR-Dataset

Following ref.[10], as shown in Fig.4 and Fig.5, construction of CrossADR-Dataset includes two stages: (1) annotation of drug combinations; (2) construction of CrossADR-DataBase and CrossADR-Dataset D and CrossADR-Dataset R (Table.1).

The CrossADR-Database is constructed through a systematic annotation process of drug pairs. During this procedure, both the ADR data and their respective sources are integrated. Initially, a pool of $1,376 \times 1,376$ possible combinations is generated based on the 1376 drugs selected for analysis. To refine this list, self-paired combinations (e.g., "drug p - drug p ") are excluded. Furthermore, the order of drugs within a pair is considered irrelevant, meaning "drug p - drug q " and "drug q - drug p " are treated as the same entity. Consequently, the total number of unique drug combinations is determined by the following calculation: $(1,376 \times 1,376 - 1,376) \times \frac{1}{2} = 946,000$.

The ADR information for these pairs is then mapped into a binary vector of length 15. This vector represents the presence or absence of ADRs across 15 specific organs, with data retrieved from the TWOSIDES and ADReCS databases. Additionally, drug-drug interactions from DrugBank are classified into three distinct categories: ADR, synergy, and others. It is important to note that DrugBank data is utilized only for auxiliary sample selection and is not involved in the actual ADR annotation. Once these steps are completed, the OrganADR-Database is finalized. All drug pairs are then categorized based on their information sources and the intersections between them. It should be noted that the data sources for positive and negative samples are determined during the construction of OrganADR-Dataset D and OrganADR-Dataset R.

In Dataset D, DrugBank records are utilized to identify negative samples. Positive samples in this dataset are defined as drug pairs recorded by TWOSIDES that are not classified as synergistic by DrugBank. Conversely, negative samples are composed of drug pairs explicitly recorded as synergistic within DrugBank. In Dataset R, a random selection method is applied to define negative samples. Here, positive samples are identified as the drug pairs documented in TWOSIDES. Negative samples are simply defined as those drug pairs that are not recorded by the TWOSIDES database.

The complete collection of positive and negative samples is not utilized for model training, validation, and testing directly. Instead, these samples function as supersets from which the specific training, validation, and testing partitions are derived, as shown below:

Let the selected set of 1,376 drugs be represented by \mathcal{V} (Fig. 5a). This set is partitioned into three mutually exclusive subsets:

$$\mathcal{V} = \mathcal{V}_{\text{train}} \cup \mathcal{V}_{\text{valid}} \cup \mathcal{V}_{\text{test}} \quad \text{and} \quad \mathcal{V}_{\text{train}} \cap \mathcal{V}_{\text{valid}} \cap \mathcal{V}_{\text{test}} = \emptyset. \quad (26)$$

Furthermore, the positive drug pair sets for training, validation, and testing are denoted by $\mathcal{C}_{\text{p-train}}$, $\mathcal{C}_{\text{p-valid}}$, and $\mathcal{C}_{\text{p-test}}$, respectively. Similarly, the negative sets are represented by $\mathcal{C}_{\text{n-train}}$, $\mathcal{C}_{\text{n-valid}}$, and $\mathcal{C}_{\text{n-test}}$. Herein, the initial positive and negative samples in CrossADR-Dataset D or R are denoted as \mathcal{S}_{p} and \mathcal{S}_{n} .

- The positive drug pairs (where at least one ADR is documented in TWOSIDES) are generated as follows:

$$\begin{cases} \mathcal{C}_{p\text{-train}} = \{(p, a_{p,q}^i, q) : p \in \mathcal{V}_{\text{train}}, q \in \mathcal{V}_{\text{train}}, (p, q) \in \mathcal{S}_p\} \\ \mathcal{C}_{p\text{-valid}} = \{(p, a_{p,q}^i, q) : p \in \mathcal{V}_{\text{valid}}, q \in \mathcal{V}_{\text{valid}}, (p, q) \in \mathcal{S}_p\} \\ \mathcal{C}_{p\text{-test}} = \{(p, a_{p,q}^i, q) : p \in \mathcal{V}_{\text{test}}, q \in \mathcal{V}_{\text{test}}, (p, q) \in \mathcal{S}_p\} \end{cases}, \quad (27)$$

- The negative drug pairs (where no ADR is documented in TWOSIDES) are generated as follows:

$$\begin{cases} \mathcal{C}_{n\text{-train}} = \{(p, a_{p,q}^i, q) : p \in \mathcal{V}_{\text{train}}, q \in \mathcal{V}_{\text{train}}, (p, q) \in \mathcal{S}_n\} \\ \mathcal{C}_{n\text{-valid}} = \{(p, a_{p,q}^i, q) : p \in \mathcal{V}_{\text{valid}}, q \in \mathcal{V}_{\text{valid}}, (p, q) \in \mathcal{S}_n\} \\ \mathcal{C}_{n\text{-test}} = \{(p, a_{p,q}^i, q) : p \in \mathcal{V}_{\text{test}}, q \in \mathcal{V}_{\text{test}}, (p, q) \in \mathcal{S}_n\} \end{cases}, \quad (28)$$

To maintain data balance, the quantity of positive drug pairs is matched with the negative drug pairs across all sets. This procedure is performed in accordance with refs.[10, 22, 30]. Statistics for the CrossADR-Dataset under random seeds are shown in Table 1.

Experiment: train and evaluate CrossADR

Loss function

Since multiple interactions between two drugs may occur, the binary cross-entropy loss is applied to the model. The loss is formulated as:

$$\mathcal{L} = -\frac{1}{15} \sum_{i=1}^{15} [a_{p,q}^i \log(\mathbf{S}_i) + (1 - a_{p,q}^i) \log(1 - \mathbf{S}_i)], \quad (29)$$

where $a_{p,q}^i$ represents the actual binary label for the i -th ADR, \mathbf{S}_i represents the predicted probability of the i -th ADR.

Optimizer

The Adam optimizer [31] is employed. Model parameters are optimized by minimizing the defined loss function.

Evaluation metrics

ROC-AUC and PR-AUC are utilized as the primary evaluation metrics. These metrics are chosen because sensitivity to the classification threshold is avoided.

- ROC-AUC:** The area under the curve is calculated for TPR vs. FPR across various threshold settings.
- PR-AUC:** The area under the curve is determined for Precision vs. Recall at different thresholds.

The constituent components are defined as:

$$\text{TPR} = \frac{\text{TP}}{\text{TP} + \text{FN}}, \quad \text{FPR} = \frac{\text{FP}}{\text{FP} + \text{TN}}, \quad (30)$$

and

$$\text{Precision} = \frac{\text{TP}}{\text{TP} + \text{FP}}, \quad \text{Recall} = \frac{\text{TP}}{\text{TP} + \text{FN}}. \quad (31)$$

For a comprehensive assessment of the classification of positive and negative samples, Accuracy, Precision, Recall, and Hamming loss are integrated as supplementary metrics.

- Accuracy:** The overall correctness. It is defined as the ratio of correctly predicted instances to the total number of samples.

$$\text{Accuracy} = \frac{\text{TP} + \text{TN}}{\text{TP} + \text{TN} + \text{FP} + \text{FN}} \quad (32)$$

- Precision:** High importance is placed on precision when false positive costs are significant. The accuracy of positive predictions:

$$\text{Precision} = \frac{\text{TP}}{\text{TP} + \text{FP}} \quad (33)$$

- Recall:** The model's ability to identify all relevant instances. This metric is prioritized when false negatives are costly.

$$\text{Recall} = \frac{\text{TP}}{\text{TP} + \text{FN}} \quad (34)$$

In these equations, TP denotes correctly identified positive cases, and TN represents correctly identified negative cases. Conversely, negative cases incorrectly labeled as positive are denoted by FP, while positive cases incorrectly identified as negative are represented by FN.

- F1-Score:** A balance between precision and recall is maintained by the F1-Score. It is calculated as the harmonic mean of the two and is frequently applied to imbalanced datasets.

$$\text{F1-Score} = 2 \times \frac{\text{Precision} \cdot \text{Recall}}{\text{Precision} + \text{Recall}} \quad (35)$$

- Hamming loss:** The fraction of incorrect labels in the multi-label task is measured by Hamming loss. The average number of misclassified labels is represented.

$$\text{Hamming loss} = \frac{1}{N \times L} \sum_{i=1}^N \sum_{j=1}^L \mathbb{I}(y_{ij} \neq \hat{y}_{ij}) \quad (36)$$

where N is defined as the total number of samples, and L is denoted as the number of labels assigned to each sample. The actual j -th label of the i -th sample is represented by y_{ij} , while the predicted label is represented by \hat{y}_{ij} . An indicator function $\mathbb{I}(y_{ij} \neq \hat{y}_{ij})$ is employed; 1 is assigned if $y_{ij} \neq \hat{y}_{ij}$, and 0 is assigned otherwise.

Results

CrossADR: organ-level adverse drug reaction prediction

Predicting ADRs for combination pharmacotherapy is a critical yet challenging task, especially for emerging drugs where historical interaction data is sparse. As illustrated in Fig.1A, the proposed CrossADR framework addresses this by formulating the problem into a multi-label classification task across 15 organs. By taking drug pairs with their molecular features as input, CrossADR maps molecular and network-level interactions to clinical ADR outcomes at the organ level. The comprehensive workflow, shown in Fig.1B-C, spans from initial drug feature extraction to the prediction of ADRs, facilitating downstream biological insights such as Protein-Protein Interaction (PPI) network mapping and pathway enrichment analysis.

Architecture of CrossADR

The CrossADR framework is designed as a hierarchical information processing pipeline that bridges the gap between microscopic drug properties and macroscopic clinical outcomes. As illustrated in Fig.1C and Fig.2, the architecture is characterized by two core innovations that distinguish it from previous GNN-KG based models like OrganADR or EmerGNN: a cross-layer feature integration strategy and a cross-level associative learning mechanism.

- Cross-layer Feature Integration:** Unlike conventional GNN architectures that rely solely on the final hidden state, CrossADR

Table 2 Overview of the KGs' edges used in this manuscript. The semantic relations, including source and target node categories, and the total edge count for each triplet type are shown. The columns "KG: Basic" and "KG: Ablation 1–3" define the corresponding edge subsets for the 4 KGs.

Relation	Type of Source Node	Type of Target Node	Number of Edges	KG: Basic	KG: Ablation 1	KG: Ablation 2	KG: Ablation 3
ppi	gene/protein	gene/protein	642,150	✓	✓		✓
associated with	effect/phenotype	gene/protein	3,330	✓	✓		
associated with	gene/protein	effect/phenotype	3,330	✓	✓		
parent-child	effect/phenotype	effect/phenotype	37,472	✓			
target	drug	gene/protein	16,380	✓	✓		✓
target	gene/protein	drug	16,380	✓	✓		✓
enzyme	drug	gene/protein	5,317	✓	✓		✓
enzyme	gene/protein	drug	5,317	✓	✓		✓
transporter	drug	gene/protein	3,092	✓	✓		✓
transporter	gene/protein	drug	3,092	✓	✓		✓
carrier	drug	gene/protein	864	✓	✓		✓
carrier	gene/protein	drug	864	✓	✓		✓
side effect	drug	effect/phenotype	64,784	✓	✓	✓	
side effect	effect/phenotype	drug	64,784	✓	✓	✓	
associated with	disease	gene/protein	80,411	✓			✓
associated with	gene/protein	disease	80,411	✓			✓
phenotype present	disease	effect/phenotype	150,317	✓		✓	
phenotype present	effect/phenotype	disease	150,317	✓		✓	
phenotype absent	disease	effect/phenotype	1,193	✓		✓	
phenotype absent	effect/phenotype	disease	1,193	✓		✓	
contraindication	disease	drug	30,675	✓		✓	✓
contraindication	drug	disease	30,675	✓		✓	✓
indication	disease	drug	9,388	✓		✓	✓
indication	drug	disease	9,388	✓		✓	✓
off-label use	disease	drug	2,568	✓		✓	✓
off-label use	drug	disease	2,568	✓		✓	✓
parent-child	disease	disease	64,388	✓		✓	✓

implements a gated-residual-flow GNN. In CrossADR, this module (Fig.2B) utilizes drug-dependent attention scores to weight the Knowledge Graph (KG) edges dynamically. By adopting a multi-scale fusion strategy, the model captures the hierarchical evolution of knowledge flow across different hop-distances in the KG. Bi-directional cross-attention is then applied to these multi-layer sequences, ensuring that the structural context of both drugs is integrated at every level of abstraction.

- **Cross-level Associative Learning:** Importantly, as shown in Fig.2E, unlike existing methods that necessitate a pre-defined label association matrix or fixed hierarchical knowledge of ADRs, CrossADR's embedding space is entirely learnable and data-driven. This approach circumvents the limitations of incomplete or biased prior medical knowledge. By allowing the model to autonomously capture latent dependencies between organ-level responses, CrossADR can identify non-obvious clinical associations that are often overlooked by rigid, manually-curated correlation structures, thereby enhancing the robustness of multi-label ADR predictions in complex pharmacotherapy scenarios.

Finally, a cross-level cross-attention module integrates these molecular-level network with the refined organ-level latent features. This dual-pathway design—processing "bottom-up" molecular information and "top-down" biological associations simultaneously—enables CrossADR to achieve superior predictive accuracy and meanwhile provides a more interpretable representation of how drug interactions manifest as specific organ-level ADRs.

Generation of different KGs

In the architecture of Graph Neural Network (GNN)-based models, the KG is recognized as an indispensable module for capturing high-order biological relationships. As information carriers, the richness and diversity of KGs are crucial for the model's representative ability. Although the focus of this study is the development of the CrossADR model's architecture, different KGs are strategically constructed to comprehensively evaluate the performance and robustness of the proposed framework under varying information densities.

As illustrated in Fig.3A, the foundational "KG: Basic" is constructed based on PrimeKG. Following the preprocessing protocols established in previous studies [22, 10], specific node types and relations associated with drug mechanisms are prioritized. The basic KG comprises four primary entity types: drug, gene/protein, effect/phenotype, and disease. As detailed in Table 2, a comprehensive network is formed with 27 types of semantic relations. Notably, Protein-Protein Interactions (PPIs) constitute the largest portion of the graph with 642,150 edges, while drug-related interactions such as "target", "enzyme", and "side effect" are integrated to provide a multi-faceted pharmacological context. Synergistic interaction edges between drugs are explicitly removed to prevent any potential knowledge leakage. In addition, 15 types of ADRs (15 organs) connecting drugs, as well as node-to-node self-loops, are also included in the final KG used for training.

Furthermore, three ablated KGs are derived from the basic version to facilitate downstream performance assessment and sensitivity analysis (Fig.3B-D). These KGs are summarized as follows:

- **KG: Ablation 1** is designed to focus on the immediate biological neighborhood of drugs. In this version, all disease-related nodes

and their associated edges (e.g., "contraindication") are removed, and only drug, protein, and phenotype nodes are retained.

- **KG: Ablation 2** is constructed to evaluate the model's performance when protein-level information is completely absent. All gene/protein nodes and their corresponding interactions, including PPIs and drug-target relations, are excluded, leaving only the clinical and phenotypic associations.
- **KG: Ablation 3** represents a configuration where phenotypic information is removed. All "effect/phenotype" nodes, "side effect" relations and other related edges are purged, focusing instead on the relationships between diseases, proteins and drugs.

These ablated KGs serve as the topological foundation for the subsequent comparative experiments, allowing for a granular understanding of how different biological knowledge components contribute to or affect on the prediction of organ-level ADRs.

Construction and statistics of CrossADR-Dataset

As shown in Fig.4 and Fig.5, the CrossADR-Dataset is constructed through a pipeline involving drug selection and multi-source annotation. The construction of CrossADR-Dataset expands the analysis to a pool of 1,376 clinically relevant drugs. As shown in Fig.5A, this results in a vast combination space of 946,000 unique drug-drug pairs. To ensure the chemical and biological representativeness of these drugs, their identifiers are cross-referenced across PrimeKG [27], TWOSIDES [26], and DrugBank [29], ensuring that all analyzed drugs possess both structural descriptors (SDFs) and network-based positions in the knowledge graph.

The annotation process (Fig.4A) maps raw ADR symptoms from TWOSIDES to 15 specific organ systems using the ADReCS [28] hierarchy. Furthermore, we integrated DrugBank's interaction records as auxiliary information to distinguish between ADR-related interactions and synergistic effects (Fig.4B). Following the methodology of OrganADR [10], two distinct benchmark datasets are established to evaluate the model under different scenarios:

- **CrossADR-Dataset D:** This dataset utilizes DrugBank's synergistic records as a high-confidence source for negative samples, while positive samples are pairs documented in TWOSIDES that are not synergistic.
- **CrossADR-Dataset R:** In this more challenging configuration, negative samples are randomly selected from the complement set of documented ADR pairs in TWOSIDES, reflecting a broader pharmacological space with uncertain annotations.

Statistical comparison (Fig.5D-E) highlights the expansion of CrossADR-Dataset. While the previous OrganADR-Dataset utilized approximately 500-600 drugs for training, the CrossADR-Dataset increases the number of training drugs to over 1,000 (e.g., an average of 1022.5 ± 3.5 for Dataset D across different random seeds and 1100 for Dataset R). This expansion is further reflected in the triplet counts; for instance, the number of triplets in the training set increased from approximately 23,749 in OrganADR to an average of $65,924.8 \pm 2109.2$ drug pairs across seed in the CrossADR-Dataset.

Drug-disjoint partitioning (8:1:1 ratio) are performed. As detailed in Table 1, the drugs are divided into $\mathcal{V}_{\text{train}}$, $\mathcal{V}_{\text{valid}}$, and $\mathcal{V}_{\text{test}}$, ensuring that drugs in the test set never appeared during training.

Comparison of CrossADR with baseline models

To evaluate the predictive performance of the proposed CrossADR framework, a comprehensive comparative analysis is conducted across two benchmark datasets (CrossADR-Dataset D and Dataset R) under four distinct Knowledge Graph (KG) configurations. The performance of CrossADR is compared against six baseline models, including two state-of-the-art deep learning architectures specifically designed for drug-drug interaction (DDI) tasks—OrganADR [10] and a modified version of EmerGNN [22]—and four traditional machine learning (ML) models: Random Forest (RF), K-Nearest Neighbors (KNN), Gaussian Naive Bayes (GNB), and Decision Tree (DT).

As summarized in Table 3, the overall performance on the foundational "KG: Basic" demonstrates that CrossADR consistently outperforms all baseline models across all five evaluation metrics. In CrossADR-Dataset D, CrossADR achieves a ROC-AUC of $83.75\% \pm 4.31\%$ and an F1-score of $75.32\% \pm 4.76\%$, representing a significant improvement over the second-best model, OrganADR (ROC-AUC: $82.76\% \pm 4.04\%$). A similar trend is observed in the more challenging CrossADR-Dataset R, where CrossADR maintains a high ROC-AUC of $83.57\% \pm 3.26\%$. Notably, the deep learning-based models (CrossADR, OrganADR, and EmerGNN) exhibit a substantial performance gap compared to traditional ML methods. For instance, the ROC-AUC of the best-performing ML model (RF) is approximately 61.31% in Dataset D, which is 22.44% lower than that of CrossADR, highlighting the necessity of integrating multi-scale biological knowledge via GNNs and the proposed architecture.

The robustness of CrossADR is further validated through significance testing across all four KG topologies, as detailed in Table 4. When compared to OrganADR and EmerGNN, CrossADR demonstrates statistically significant improvements in nearly every scenario. On the Basic KG, the P -values for ROC-AUC compared to OrganADR are 2.24×10^{-3} and 9.75×10^{-11} for Dataset D and R, respectively. Even under information-sparse conditions (Ablations 1–3), where performance generally declines for all models due to the removal of disease, protein, or phenotype nodes, CrossADR remains the superior model. For example, in KG: Ablation 2 (where protein information is removed), CrossADR achieves a mean ROC-AUC of 69.6% (Dataset D) and 70.2% (Dataset R), outperforming OrganADR by 4.9% and 3.8%, respectively, with high significance ($P < 0.001$). The effect sizes (Cohen's d) are notably high, reaching 1.690 in the Dataset R Basic KG scenario, indicating that the architectural innovations of CrossADR—specifically the cross-layer integration and learnable ADR embeddings—provide substantial gains that are not dependent on specific KG densities.

The comprehensive performance distribution is visually illustrated in Fig. 6, which presents the results of 60 independent experimental runs for the deep learning models and 10 runs for the ML models. The boxplots reveal that CrossADR not only achieves higher median values but also maintains relatively narrow interquartile ranges, suggesting high stability across different data partitions. In Fig. 6A (KG: Basic), the ROC-AUC and F1-score distributions for CrossADR are shifted significantly upward compared to EmerGNN and the ML baselines. As the KG complexity decreases from Fig. 6B to 6D, while the absolute performance of all models is impacted by the loss of topological information, CrossADR consistently maintains its lead. Specifically, in KG: Ablation 3 (Fig. 6D), where phenotypic information is absent, the median F1-score of CrossADR in Dataset D (59.75%) remains higher than that of OrganADR (56.54%)

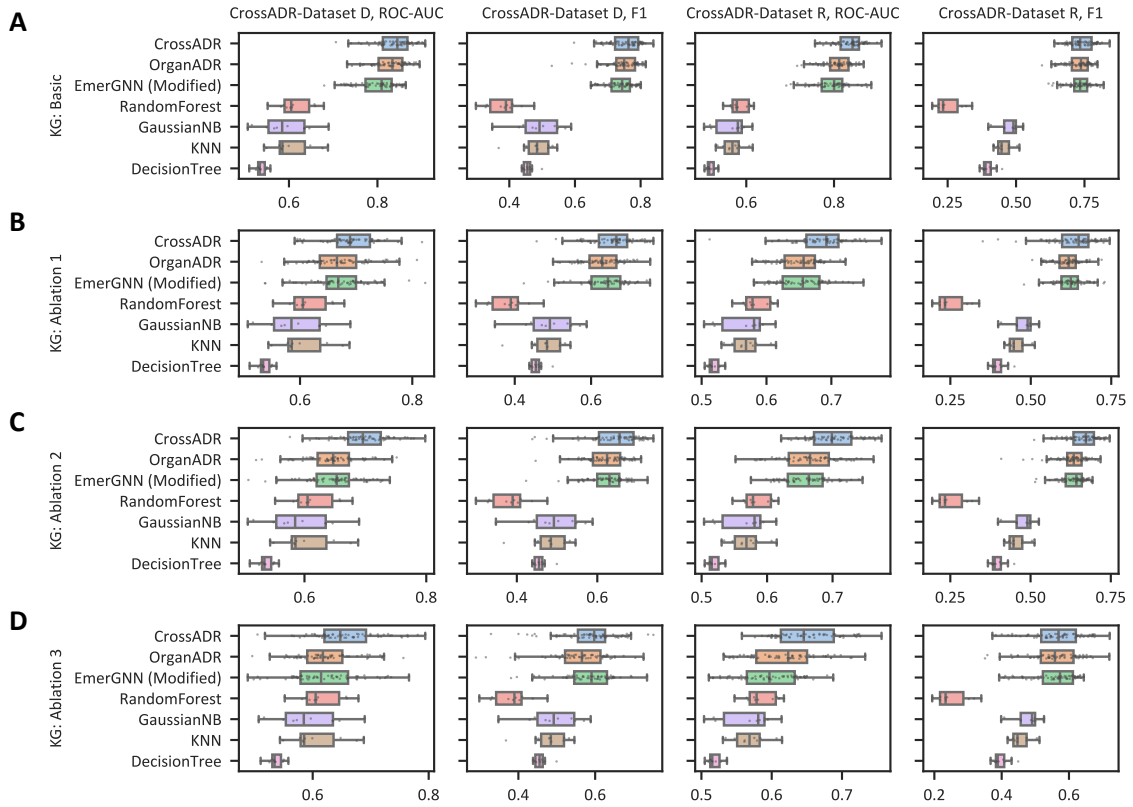


Figure 6 Performance comparison of CrossADR against baseline models. The figure is organized into a 4×4 panel matrix: rows 1 to 4 correspond to different Knowledge Graph configurations (KG: Basic, KG: Ablation 1, KG: Ablation 2, and KG: Ablation 3, respectively); the first two columns present results for CrossADR-Dataset D (ROC-AUC and F1-score), while the last two columns show results for CrossADR-Dataset R (ROC-AUC and F1-score). In each boxplot, individual scatter points represent results from independent experimental runs, the central horizontal line indicates the median value, the box boundaries denote the upper and lower quartiles, and the whiskers extend to illustrate the overall data range excluding outliers. For each model in each subplot, $N = 60$.

Table 3 Performance of CrossADR with baseline models across 5 metrics. CrossADR, OrganADR and EmerGNN are run three times with random seeds 10, 20, 30. Four ML models are run one time with fixed random state 1. The process above is repeated on ten datasets, which are generated with the random seeds 10, 15, 20, 25, 30, 35, 40, 45, 50 and 55. Given that the ratio of validation set to test set is 1:1, the two sets serve as mutual validation and test sets, and are tested twice. The reported values in table are the mean value and standard deviation calculated from a total of 60 runs for deep-learning models and 10 runs for machine-learning models. All evaluation metrics are shown as percentages (%), where higher values are better for ROC-AUC, PR-AUC, ACC and F1, and lower values indicate better performance for HL. Best results in **bold**, second best underlined.

Datasource	Model	PR-AUC	ROC-AUC	ACC	F1	HL
CrossADR-Dataset D	CrossADR	$83.83\% \pm 3.99\%$	$83.75\% \pm 4.31\%$	$76.44\% \pm 3.91\%$	$75.32\% \pm 4.76\%$	$24.25\% \pm 3.93\%$
	OrganADR	$83.17\% \pm 4.25\%$	$82.76\% \pm 4.04\%$	$75.34\% \pm 3.87\%$	$74.52\% \pm 5.32\%$	$24.66\% \pm 3.87\%$
	EmerGNN (Modified)	$81.57\% \pm 4.32\%$	$79.86\% \pm 4.51\%$	$72.71\% \pm 4.68\%$	$73.69\% \pm 4.13\%$	$27.29\% \pm 4.68\%$
	RandomForest	$61.94\% \pm 4.68\%$	$61.31\% \pm 3.98\%$	$56.14\% \pm 2.59\%$	$38.37\% \pm 5.35\%$	$43.86\% \pm 2.59\%$
	KNN	$58.20\% \pm 4.05\%$	$60.35\% \pm 5.03\%$	$56.91\% \pm 3.04\%$	$48.28\% \pm 5.23\%$	$43.09\% \pm 3.04\%$
	GaussianNB	$57.76\% \pm 5.26\%$	$59.14\% \pm 5.96\%$	$56.98\% \pm 5.19\%$	$49.20\% \pm 7.34\%$	$43.02\% \pm 5.19\%$
	DecisionTree	$52.10\% \pm 0.84\%$	$53.59\% \pm 1.36\%$	$53.58\% \pm 1.36\%$	$45.73\% \pm 1.82\%$	$46.42\% \pm 1.36\%$
CrossADR-Dataset R	CrossADR	$82.91\% \pm 3.33\%$	$83.57\% \pm 3.26\%$	$75.45\% \pm 3.15\%$	$74.06\% \pm 4.40\%$	$25.24\% \pm 3.12\%$
	OrganADR	$79.79\% \pm 3.48\%$	$80.67\% \pm 3.31\%$	$73.25\% \pm 3.17\%$	$72.76\% \pm 4.55\%$	$26.75\% \pm 3.17\%$
	EmerGNN (Modified)	$79.26\% \pm 3.82\%$	$79.42\% \pm 4.09\%$	$72.61\% \pm 3.80\%$	$73.16\% \pm 4.27\%$	$27.39\% \pm 3.80\%$
	RandomForest	$58.91\% \pm 3.51\%$	$58.47\% \pm 2.32\%$	$53.71\% \pm 1.70\%$	$24.86\% \pm 5.22\%$	$46.29\% \pm 1.70\%$
	GaussianNB	$55.42\% \pm 2.87\%$	$56.59\% \pm 3.81\%$	$55.22\% \pm 2.49\%$	$47.48\% \pm 4.44\%$	$44.78\% \pm 2.49\%$
	KNN	$54.96\% \pm 2.03\%$	$56.95\% \pm 2.82\%$	$54.31\% \pm 1.92\%$	$45.68\% \pm 3.33\%$	$45.69\% \pm 1.92\%$
	DecisionTree	$51.12\% \pm 0.61\%$	$51.92\% \pm 1.08\%$	$51.91\% \pm 1.08\%$	$39.83\% \pm 2.51\%$	$48.09\% \pm 1.08\%$

and EmerGNN (59.06%), demonstrating the CrossADR’s ability to effectively leverage cross-level information through its gated-residual-flow mechanism and associative learning architectures.

CrossADR’s performance across 15 organs

To further evaluate the fine-grained predictive capability of the proposed model, the performance of CrossADR is assessed across 15 specific organ categories. This granular analysis is conducted to

Table 4 Significance test of CrossADR with baseline model OrganADR and EmerGNN. Consistent with the previous annotation, the reported values in table are calculated from a total of 60 runs. The values reported for Model 1 and Model 2 represent the mean ROC-AUC across experimental runs. ** ($P < 0.01$), *** ($P < 0.001$). Note that EmerGNN implemented in this comparison is the Modified EmerGNN adapted in this manuscript.

Dataset	KG	CrossADR (Model 1) vs OrganADR (Model 2)					CrossADR (Model 1) vs EmerGNN (Model 2)				
		Model 1	Model 2	P-Value	Sig	Effect Size	Model 1	Model 2	P-Value	Sig	Effect Size
CrossADR Dataset-D	Basic	83.7%	82.8%	2.24×10^{-3}	**	0.413	83.7%	79.9%	8.96×10^{-15}	***	1.327
	Ablation 1	68.8%	66.9%	2.74×10^{-3}	**	0.404	68.8%	66.9%	1.91×10^{-3}	**	0.420
	Ablation 2	69.6%	64.7%	1.18×10^{-11}	***	1.084	69.6%	64.8%	8.99×10^{-11}	***	1.016
	Ablation 3	65.5%	62.4%	1.11×10^{-4}	***	0.535	65.5%	62.2%	6.01×10^{-4}	***	0.468
CrossADR Dataset-R	Basic	83.6%	80.7%	9.75×10^{-11}	***	1.690	83.6%	79.4%	1.22×10^{-18}	***	1.650
	Ablation 1	68.4%	65.2%	1.21×10^{-8}	***	0.734	68.4%	65.4%	3.50×10^{-7}	***	0.651
	Ablation 2	70.2%	66.4%	1.65×10^{-10}	***	0.996	70.2%	66.0%	9.75×10^{-11}	***	1.435
	Ablation 3	65.1%	61.9%	4.49×10^{-6}	***	0.652	65.1%	59.7%	1.45×10^{-12}	***	1.154

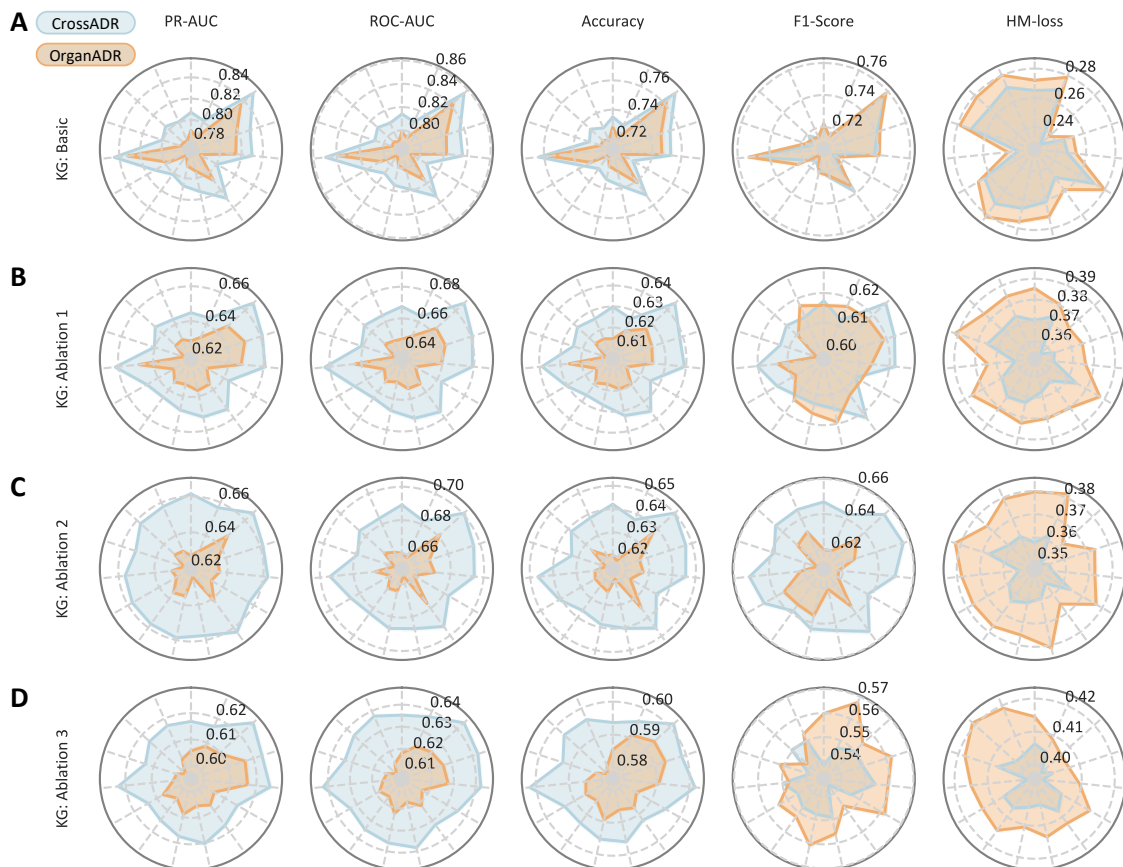


Figure 7 Evaluation of CrossADR versus OrganADR across 15 organs. (A-D) Comprehensive evaluation across four KG configurations (Basic and Ablations 1–3) using five metrics: PR-AUC, ROC-AUC, Accuracy, F1-Score, and Hamming Loss (HM-loss). Each of the 15 axes represents a specific organ category.

verify whether the architectural advantages of CrossADR translate into consistent improvements across diverse physiological systems. As illustrated in Fig.7, the performance of CrossADR is compared against the previously state-of-the-art OrganADR model using five metrics (PR-AUC, ROC-AUC, Accuracy, F1-Score, and Hamming Loss) under four distinct Knowledge Graph (KG) configurations. In each radar chart, the 15 axes represent individual organ systems, providing a multi-dimensional visualization of the models' robustness.

As shown in Fig.7A, under the "KG: Basic", CrossADR demonstrates a consistent lead over OrganADR across all 15 organs. For the PR-AUC metric, CrossADR achieves values ranging from

80.07% to 85.08%, whereas OrganADR yields lower values between 77.96% and 83.53%. Specifically, in Organ 3, CrossADR reaches a peak PR-AUC of 85.08%, surpassing OrganADR's 83.53%. A similar trend is observed in ROC-AUC, where CrossADR maintains a range of 80.82% to 85.54%, consistently outperforming OrganADR (79.02% to 84.30%). Regarding prediction accuracy, CrossADR records a minimum of 72.87% (Organ 6) and a maximum of 76.99% (Organ 3), while the accuracy of OrganADR remains consistently lower, with a range of 71.81% to 76.21%. Notably, the HM-loss of CrossADR is reduced. For instance, in Organ 3, CrossADR achieves the lowest HM-loss of 23.01%, whereas OrganADR records 23.79%.

Table 5 Significance test of CrossADR with two ablation studies. Consistent with the previous annotation, the reported values in table are calculated from a total of 60 runs. The values reported for Model 1 and Model 2 represent the mean ROC-AUC across experimental runs. * ($P < 0.05$), ** ($P < 0.01$), *** ($P < 0.001$). Ablation 1 and Ablation 2 refer to ablated variants of CrossADR, with detailed information in the main text.

Dataset	KG	CrossADR (Model 1) vs Ablated 1 (Model 2)					CrossADR (Model 1) vs Ablated 2 (Model 2)				
		Model 1	Model 2	P-Value	Sig	Effect Size	Model 1	Model 2	P-Value	Sig	Effect Size
CrossADR Dataset-D	Basic	83.7%	82.4%	9.29×10^{-6}	***	0.626	83.7%	81.8%	1.74×10^{-6}	***	0.686
	Ablation 1	68.8%	67.4%	1.22×10^{-4}	***	0.450	68.8%	67.3%	8.56×10^{-3}	**	0.351
	Ablation 2	69.6%	67.6%	1.00×10^{-3}	***	0.451	69.6%	65.4%	7.23×10^{-9}	***	0.871
	Ablation 3	65.5%	64.0%	1.31×10^{-2}	*	0.330	65.5%	62.1%	9.81×10^{-5}	***	0.540
CrossADR Dataset-R	Basic	83.6%	81.7%	7.47×10^{-12}	***	1.099	83.6%	80.9%	1.24×10^{-10}	***	1.006
	Ablation 1	68.4%	67.0%	1.36×10^{-5}	***	0.465	68.4%	66.0%	2.64×10^{-6}	***	0.613
	Ablation 2	70.2%	69.1%	6.02×10^{-5}	***	0.545	70.2%	66.0%	2.84×10^{-9}	***	1.000
	Ablation 3	65.1%	63.8%	1.00×10^{-3}	***	0.368	65.1%	61.1%	5.55×10^{-8}	***	0.961

The superiority of CrossADR is maintained even under information-sparse conditions provided by the ablated KGs. As illustrated in Fig.7B–D, although the absolute performance of both models declines when biological nodes (diseases, proteins, or phenotypes) are removed, CrossADR consistently encompasses a larger area in the radar charts than OrganADR. In the "KG: Ablation 2" scenario (Fig.7C), where protein information is absent, CrossADR still achieves an ROC-AUC of 70.08% in Organ 3, which is 1.94% higher than the 68.14% achieved by OrganADR. Furthermore, in the "KG: Ablation 3" configuration (Fig.7D), where phenotypic information is removed, CrossADR maintains an F1-score between 53.58% and 55.41%, whereas OrganADR's performance fluctuates between 54.19% and 56.74% with higher instability across organs.

Ablation study

To evaluate the contributions of the proposed modules within the CrossADR framework, a comprehensive ablation study is conducted. The analysis focuses on two primary architectural innovations: the cross-layer GNN on the Knowledge Graph (KG) and the cross-level attention module with a learnable ADR embedding space. Two ablated variants are developed for comparison. In Ablated 1, the cross-level attention module is replaced by the ADR association matrix approach used in OrganADR, while the cross-layer GNN module is retained. In Ablated 2, the cross-layer GNN is replaced with the traditional GNN structure found in OrganADR and EmerGNN, but the matrix-free learnable embedding module is maintained.

The quantitative results across different KGs and datasets are summarized in Table 5. The full CrossADR model (Model 1) consistently outperformed both ablated variants with high statistical significance. On the foundational "KG: Basic" of CrossADR Dataset-D, the ROC-AUC of CrossADR reached 83.7%. In contrast, the performance of Ablated 1 and Ablated 2 dropped to 82.4% ($P = 9.29 \times 10^{-6}$) and 81.8% ($P = 1.74 \times 10^{-6}$), respectively. These results indicate that both the multi-scale knowledge flow and the associative learning mechanism are essential for optimal prediction.

A similar trend is observed in CrossADR Dataset-R. On the Basic KG, the ROC-AUC of the full model (83.6%) is significantly higher than that of Ablated 1 (81.7%) and Ablated 2 (80.9%). Notably, the effect sizes for these comparisons reached 1.099 and 1.006, respectively. This suggests that the removal of either module leads to a substantial loss in the model's representative capability.

The superiority of the full architecture is also maintained under information-sparse conditions. For instance, in the "KG: Ablation

2" scenario for Dataset-D, CrossADR achieved a mean ROC-AUC of 69.6%. This represents a lead of 2.0% over Ablated 1 (67.6%) and 4.2% over Ablated 2 (65.4%). The performance degradation is most pronounced in Ablated 2 across most KGs, highlighting that the cross-layer GNN module plays a dominant role in capturing complex drug interactions. Overall, the ablation study confirms that the synergy between hierarchical feature integration and latent organ-level associations is fundamental to the robustness of CrossADR.

Identification of key PPIs and pathways with CrossADR

To demonstrate the practical utility and interpretability of the CrossADR framework, a case study is conducted on a representative drug combination: Donepezil (an acetylcholinesterase inhibitor) and Benztropine (a muscarinic antagonist), as shown in Fig.8A. This drug pair represents a classic scenario of cholinergic imbalance. In clinical practice, Donepezil is utilized to increase acetylcholine levels for the treatment of Alzheimer's disease, while Benztropine is administered to block acetylcholine receptors to alleviate extrapyramidal symptoms. The pharmacological conflict between these two agents—one acting as a "cholinergic booster" and the other as a "cholinergic blocker"—would create a severe "tug-of-war" within the autonomic and central nervous systems in human's body[32].

As illustrated in Fig.8B, the predictive capability of CrossADR is evaluated. For this specific drug pair, clinical records indicate the occurrence of adverse drug reactions (ADRs) in 12 distinct organs, including the brain, heart, liver, kidney, and intestine. The prediction results show that CrossADR accurately identifies the ADR status for all 12 organs, achieving 100% accuracy. This high degree of alignment with clinical data suggests that the model effectively captures the ADRs arising from the antagonistic interaction of the two drugs.

To further investigate the mechanism underlying these multi-organ ADRs, CrossADR is utilized to prioritize the most influential proteins. Eight key proteins are identified: CHRM1, CHRM2, CHRM3, CHRM4, CHRM5, LYNX1, PRIMA1, and GNRHR. A PPI network is visualized in Fig.8C, showing the dense functional connectivity between these targets. Notably, the muscarinic acetylcholine receptors (CHRM1–5) are identified as the core mediators, which is consistent with the known pharmacology where Benztropine directly competes with the increased acetylcholine (facilitated by Donepezil) at these sites. Additionally, proteins like PRIMA1, which anchors acetylcholinesterase to neuronal membranes, and LYNX1, a modulator of nicotinic receptors, are identified as critical nodes in the protein-protein-interaction network[33].

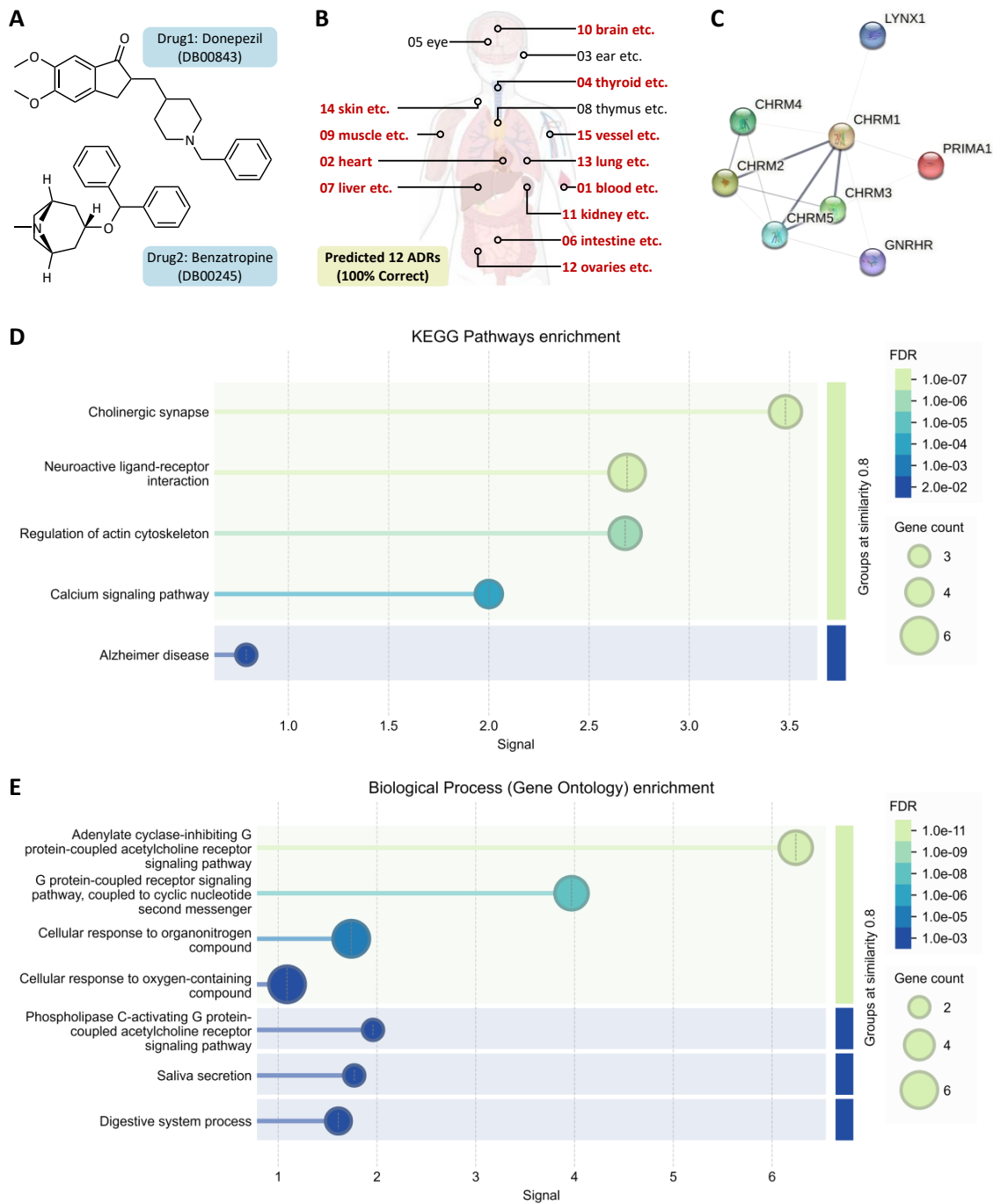


Figure 8 Case study and interpretability analysis of CrossADR. (A) Drug combination to be analyzed: Drug 1, Donepezil and Drug 2, Benztropine. (B) Predicted ADRs for the drug combination. (C) Visualization of the PPI network. The proteins in the PPI network are identified as important proteins by CrossADR. (D) KEGG pathway enrichment analysis of the key proteins. (E) Gene Ontology (GO) Biological Process enrichment analysis of the key proteins.

The biological relevance of these identified proteins is further validated through enrichment analysis. As shown in the KEGG pathway enrichment (Fig.8D), the "Cholinergic synapse" and "Neuroactive ligand-receptor interaction" pathways are the most significantly enriched. This matches the biological expectation that the ADRs are primarily driven by the disruption of cholinergic transmission. Furthermore, the Gene Ontology (GO) Biological Process analysis (Fig.8E) reveals high enrichment in the "Adenylate cyclase-inhibiting G protein-coupled acetylcholine receptor signaling

pathway" and "Phospholipase C-activating G protein-coupled acetylcholine receptor signaling pathway." These pathways directly correspond to the downstream signaling of M2/M4 and M1/M3/M5 receptors, respectively. The mechanisms identified by CrossADR are strongly supported by established pharmacological knowledge. For example, the disruption of M3 receptors in the intestine and bladder is known to cause gastrointestinal motility disorders and urinary retention[34], while the interference with M2 receptors in the heart is associated with conduction disturbances. The successful

identification of these proteins and pathways demonstrates that CrossADR not only provides accurate organ-level predictions but also offers a high-resolution, biological interpretation of the molecular mechanisms driving complex ADRs with drug combination.

Discussion

In this study, the CrossADR framework is introduced to address the challenge of organ-level adverse drug reaction prediction in combination pharmacotherapy. The model is rigorously evaluated on the newly constructed CrossADR-Dataset, which represents a significant expansion in drug combination space. Results indicate that CrossADR consistently achieves superior performance compared to state-of-the-art architectures and traditional machine learning methods across various knowledge graph configurations [7, 15]. The effectiveness of the proposed architectural innovations is verified through comprehensive ablation studies and fine-grained cross-organ analysis. Furthermore, the practical utility of the framework is demonstrated through case studies that successfully identify key proteins and biological pathways, providing high-resolution interpretability for complex clinical outcomes [8, 18].

The primary innovation of CrossADR lies in the departure from traditional, fixed adverse drug reaction association matrices that often reflect inherent training data biases. Instead, a learnable ADR embedding space is implemented to capture organ-level information dynamically. This approach enhances cross-dataset generalization and flexibility by allowing the model to focus on interpretable biological knowledge rather than dataset-specific distributions [16, 17]. Technically, the architecture emphasizes cross-layer feature integration within the gated-residual-flow module to fuse molecular features throughout the biomedical network. Cross-level associative learning is achieved through bi-directional cross-attention and gated mechanisms, which effectively bridge the gap between microscopic molecular signals and macroscopic organ-level responses.

The performance gains are attributed to the model's ability to mitigate deficiencies identified in previous architectures. Earlier models often treat molecular and organ information as isolated components or rely on simple attention that fails to capture the multi-scale evolution of knowledge flow. CrossADR addresses this by integrating vital information across different biological scales through deep feature fusion. By utilizing gated modules and residual connections, structural feature homogenization and numerical over-smoothing are prevented, ensuring that initial drug identities are preserved during deep propagation. Unlike models restricted by rigid, manually-curated correlation structures, the flexible associative learning mechanism allows for the identification of non-obvious clinical associations, such as those demonstrated in our cholinergic case study involving specific muscarinic receptor structures [34, 33, 32].

Despite these advancements, several limitations are recognized that suggest directions for future work. The predictive accuracy remains partially dependent on the completeness and quality of the underlying biomedical knowledge graph [13, 35]. Additionally, the current framework is designed for binary classification and does not explicitly account for the severity or dose-dependent nature of adverse reactions. Future research will focus on the integration of single-cell data and longitudinal patient records to further refine personalized risk assessments [36, 37]. Enhancing the model to handle multi-modal

inputs and temporal physiological changes is expected to improve the clinical utility of the system for real-world medication management and the training of next-generation bioinformatics experts [21, 11].

Conclusion

In this study, CrossADR is presented as a hierarchical framework designed for organ-level adverse drug reaction prediction through the integration of cross-layer feature fusion and cross-level associative learning. By utilizing a gated-residual-flow graph neural network and a learnable ADR embedding space, the model effectively captures the multi-scale dependencies between microscopic molecular interactions and macroscopic physiological responses across 15 organs. Evaluations on the comprehensive CrossADR-Dataset demonstrate that superior performance is consistently achieved over existing state-of-the-art methods in diverse clinical scenarios. Furthermore, the biological interpretability of the framework is confirmed through the identification of key protein-protein interactions and metabolic pathways, suggesting that CrossADR serves as a robust and reliable tool for enhancing safety assessments in combination pharmacotherapy and supporting precision clinical decision-making, drug safety as well as drug management.

Conflicts of interest

The authors declare that they have no competing interests.

References

1. Zohar B Weinstein, Nurdan Kuru, Szilvia Kiriakov, Adam C Palmer, Ahmad S Khalil, Paul A Clemons, Muhammad H Zaman, Frederick P Roth, and Murat Cokol. Modeling the impact of drug interactions on therapeutic selectivity. *Nature communications*, 9(1):3452, 2018.
2. Chachrit Khunsriraksakul, Daniel McGuire, Renan Sauteraud, Fang Chen, Lina Yang, Lida Wang, Jordan Hughey, Scott Eckert, J Dylan Weissenkampen, Ganesh Shenoy, et al. Integrating 3d genomic and epigenomic data to enhance target gene discovery and drug repurposing in transcriptome-wide association studies. *Nature communications*, 13(1):3258, 2022.
3. Akiko Iwasaki and Yexin Yang. The potential danger of suboptimal antibody responses in covid-19. *Nature Reviews Immunology*, 20(6):339–341, 2020.
4. Eva Montané and Javier Santesmases. Reacciones adversas a medicamentos. *Medicina clinica*, 154(5):178–184, 2020.
5. Jacqueline C Bouvy, Marie L De Bruin, and Marc A Koopmanschap. Epidemiology of adverse drug reactions in europe: a review of recent observational studies. *Drug safety*, 38:437–453, 2015.
6. Parvati B Patel and Tejas K Patel. Mortality among patients due to adverse drug reactions that occur following hospitalisation: a meta-analysis. *European Journal of Clinical Pharmacology*, 75:1293–1307, 2019.
7. Jingtong Wan, Chenyang Jia, Danhong Dong, Yigang Chen, Yang-Chi-Dung Lin, Yisheng He, Hsi-Yuan Huang, and Hsien-Da Huang. Deepadr: multimodal prediction of adverse drug reaction frequency by integrating early-stage drug discovery information via kolmogorov–arnold networks. *Briefings in Bioinformatics*, 26(6):bbaf695, 2025.
8. Yang Gao, Xiang Zhang, Zhongquan Sun, Payal Chandak, Jiajun Bu, and Haishuai Wang. Precision adverse drug reactions

- prediction with heterogeneous graph neural network. *Advanced Science*, 12(4):2404671, 2025.
9. Karen O’Leary. A genetic test to predict adverse drug reactions. *Nature Medicine*, 2023.
 10. Boyang Li, Yifan Qi, Bo Li, and Xiaoqiong Li. Predicting adverse drug reactions for combination pharmacotherapy with cross-scale associative learning via attention modules. *Nature Computational Science*, 5(7):547–561, 2025.
 11. Cheng Chen, Thanh Phuong Pham Nguyen, John E Hughes, Sean Hennessy, Charles E Leonard, Todd A Miano, Antonios Douros, Joshua J Gagne, and Katsiaryna Bykov. Evaluation of drug–drug interactions in pharmacoepidemiologic research. *Pharmacoepidemiology and Drug Safety*, 34(1):e70088, 2025.
 12. Guihong Wan, Wenxin Chen, Sara Khattab, Katie Roster, Nga Nguyen, Boshen Yan, Ahmad Rajeh, Jayhyun Seo, Hannah Rashdan, Leyre Zubiri, et al. Multi-organ immune-related adverse events from immune checkpoint inhibitors and their downstream implications: a retrospective multicohort study. *The Lancet Oncology*, 25(8):1053–1069, 2024.
 13. Yao Tian, Jiakai Yi, Ningning Wang, Chengkun Wu, Jinfu Peng, Shao Liu, Guoping Yang, and Dongsheng Cao. Ddinter 2.0: an enhanced drug interaction resource with expanded data coverage, new interaction types, and improved user interface. *Nucleic Acids Research*, 53(D1):D1356–D1362, 2025.
 14. Charlotte Harrison. Predicting adverse drug reactions. *Nature Reviews Drug Discovery*, 11(2):108–108, 2012.
 15. Mengli Li, Chao Cao, Quan Zou, Leyi Wei, and Yansu Wang. Mhafr-ddi: a multimodal hierarchical attention fusion and relation-aware architecture for drug–drug interaction event prediction. *Briefings in Bioinformatics*, 27(1):bbag077, 2026.
 16. Jinlu Zhang, Xuting Zhang, Yizheng Dai, Xin Shao, and Xiaohui Fan. Transformer-based graphs for drug–drug interaction with chemical knowledge embedding. *Briefings in Bioinformatics*, 27(1):bbag039, 2026.
 17. Dongxu Li, Yue Yang, Ziwen Cui, Hengchuang Yin, Pengwei Hu, and Lun Hu. Llm-ddi: leveraging large language models for drug–drug interaction prediction on biomedical knowledge graph. *IEEE Journal of Biomedical and Health Informatics*, 2025.
 18. Zhonghao Ren, Xiangxiang Zeng, Yizhen Lao, Zhuhong You, Yifan Shang, Quan Zou, and Chen Lin. Predicting rare drug–drug interaction events with dual-granular structure-adaptive and pair variational representation. *Nature Communications*, 16(1):3997, 2025.
 19. Xiaorui Su, Lun Hu, Zhuhong You, Pengwei Hu, and Bowei Zhao. Attention-based knowledge graph representation learning for predicting drug–drug interactions. *Briefings in bioinformatics*, 23(3):bbac140, 2022.
 20. Haochen Zhao, Peng Ni, Qichang Zhao, Xiao Liang, Di Ai, Shannon Erhardt, Jun Wang, Yaohang Li, and Jianxin Wang. Identifying the serious clinical outcomes of adverse reactions to drugs by a multi-task deep learning framework. *Communications Biology*, 6(1):870, 2023.
 21. Daudi Jjingo, Andrew Walakira, Suhaila Hashim, Cisse Cheickna, Ronald Galiwango, Caleb Kibet, Florence N Kivunike, Gerald Mboowa, Fredrick Elishama Kakembo, Babajide Ayodele, et al. Pathways, outputs and impact of nih-supported bioinformatics and genomics graduate trainees in africa. *Briefings in bioinformatics*, 27(1):bbag046, 2026.
 22. Yongqi Zhang, Quanming Yao, Ling Yue, Xian Wu, Ziheng Zhang, Zhenxi Lin, and Yefeng Zheng. Emerging drug interaction prediction enabled by a flow-based graph neural network with biomedical network. *Nature Computational Science*, 3(12):1023–1033, 2023.
 23. Arnold K Nyamabo, Hui Yu, and Jian-Yu Shi. Ssi-ddi: substructure–substructure interactions for drug–drug interaction prediction. *Briefings in Bioinformatics*, 22(6):bbab133, 2021.
 24. Hui Yu, ShiYu Zhao, and JianYu Shi. Stnn-ddi: a substructure-aware tensor neural network to predict drug–drug interactions. *Briefings in Bioinformatics*, 23(4):bbac209, 2022.
 25. Xinyu Zhu, Yongliang Shen, and Weiming Lu. Molecular substructure-aware network for drug–drug interaction prediction. In *Proceedings of the 31st ACM International Conference on Information & Knowledge Management*, pages 4757–4761, 2022.
 26. Nicholas P Tatonetti, Patrick P Ye, Roxana Daneshjou, and Russ B Altman. Data-driven prediction of drug effects and interactions. *Science translational medicine*, 4(125):125ra31–125ra31, 2012.
 27. Payal Chandak, Kexin Huang, and Marinka Zitnik. Building a knowledge graph to enable precision medicine. *Scientific Data*, 10(1):67, 2023.
 28. Qi-Xuan Yue, Ruo-Fan Ding, Wei-Hao Chen, Lv-Ying Wu, Ke Liu, and Zhi-Liang Ji. Mining real-world big data to characterize adverse drug reaction quantitatively: Mixed methods study. *Journal of Medical Internet Research*, 26:e48572, 2024.
 29. Craig Knox, Mike Wilson, Christen M Klinger, Mark Franklin, Eponine Oler, Alex Wilson, Allison Pon, Jordan Cox, Na Eun Chin, Seth A Strawbridge, et al. Drugbank 6.0: the drugbank knowledgebase for 2024. *Nucleic acids research*, 52(D1):D1265–D1275, 2024.
 30. Yue Yu, Kexin Huang, Chao Zhang, Lucas M Glass, Jimeng Sun, and Cao Xiao. Sumgnn: multi-typed drug interaction prediction via efficient knowledge graph summarization. *Bioinformatics*, 37(18):2988–2995, 2021.
 31. Diederik P Kingma and Jimmy Ba. Adam: A method for stochastic optimization. *arXiv preprint arXiv:1412.6980*, 2014.
 32. Kaycee M Sink, Joseph Thomas III, Huiping Xu, Bruce Craig, Steven Kritchevsky, and Laura P Sands. Dual use of bladder anticholinergics and cholinesterase inhibitors: Long-term functional and cognitive outcomes. *Journal of the American Geriatrics Society*, 56(5):847–853, 2008.
 33. Anselme L Perrier, Jean Massoulié, and Eric Krejci. Prima: the membrane anchor of acetylcholinesterase in the brain. *Neuron*, 33(2):275–285, 2002.
 34. Andrew C Kruse, Jianxin Hu, Albert C Pan, Daniel H Arlow, Daniel M Rosenbaum, Erica Rosemond, Hillary F Green, Tong Liu, Pil Seok Chae, Ron O Dror, et al. Structure and dynamics of the m3 muscarinic acetylcholine receptor. *Nature*, 482(7386):552–556, 2012.
 35. Shuangjia Zheng, Jiahua Rao, Ying Song, Jixian Zhang, Xianglu Xiao, Evandro Fei Fang, Yuedong Yang, and Zhangming Niu. Pharmkg: a dedicated knowledge graph benchmark for biomedical data mining. *Briefings in bioinformatics*, 22(4):bbaa344, 2021.
 36. Claudia Langenberg, Aroon D Hingorani, and Christopher JM Whitty. Biological and functional multimorbidity—from mechanisms to management. *Nature Medicine*, 29(7):1649–1657, 2023.
 37. Søren T Skou, Frances S Mair, Martin Fortin, Bruce Guthrie, Bruno P Nunes, J Jaime Miranda, Cynthia M Boyd, Sanghamitra Pati, Sally Mtenga, and Susan M Smith. Multimorbidity. *Nature Reviews Disease Primers*, 8(1):48, 2022.